Smart Structures and Systems, *Vol. 27, No. 5 (2021) 819-836*
DOI: https://doi.org/10.12989/sss.2021.27.5.819

Energy dissipation by friction for sliding blocks subjected to near-fault seismic base motion

Pablo M. Barlek Mendoza [1], Daniel Ambrosini*[2,3] and Bibiana M. Luccioni [1,3b]

[1] *Instituto de Estructuras, Universidad Nacional de Tucumán, 1800 Independencia Avenue, República Argentina*
[2] *Universidad Nacional de Cuyo, Facultad de Ingeniería, Mendoza, República Argentina*
[3] *Consejo Nacional de Investigaciones Científicas y Técnicas, República Argentina*

(*Received July 15, 2020, Revised January 2, 2021, Accepted January 25, 2021*)

Abstract. The objective of this study was to determine friction ratios that maximize energy dissipation on a seismic damper. The aforementioned friction damper basically consists of mass blocks that are able to slide on a flat surface. To carry out this analysis, a numerical-experimental approach was used. Firstly, the theoretical background and equations of motion for a SDOF system consisting of a mass supported on a flat surface with friction are introduced. Special emphasis is made on the fundamentals of stick-slip motion as well as energy considerations. Secondly, experimental studies carried out on a shaking table with harmonic and seismic records are described. These tests consisted of lead blocks contained on a U-shaped channel type aluminum section with its open end facing upwards. This configuration allowed blocks to slide solely in the direction of the base motion. Five different types of contact interfaces were considered to determine potential friction coefficients for the damper's design. Additionally, computational models based on rigid-body dynamics are presented. Numerical results were satisfactory particularly when comparing model's dissipated energy with empirical results. An analysis was carried out by calculating dissipated energy for the experimentally-calibrated models with varying friction ratios. For this purpose, eight near-fault seismic records were selected. Intervals with friction coefficients that maximize energy dissipation are proposed for each record. Finally, relationships between the computed friction ratios and register's peak ground acceleration (PGA) and root mean square acceleration (RMS) are discussed.

Keywords: friction; stick-slip motion; energy dissipation; near-fault earthquakes

1. Introduction

One of the most well-known sources of energy dissipation is the work carried out by friction forces. These forces arise as the result of relative motion between two contacting surfaces. Several passive vibration control devices rely on this basic principle to reduce relevant response parameters in structural systems, such as accelerations and displacements.

Limited slip bolted joints (Pall *et al*. 1980) and energy dissipating restraints (Nims *et al*. 1993) are two type of friction dampers that have been implemented on structures to improve seismic performance. These and other friction-based devices have been extensively studied and greatly improved over the years (Lee *et al*. 2008, Zahraei *et al*. 2013, Shen *et al*. 2017 and Ontiveros-Perez *et al*. 2019).

On the other hand, friction tuned mass dampers (FTMDs) (Inaudi and Kelly 1995, Ricciardelli and Vickery 1999) are becoming more popular in recent literature (Kim and Lee 2019). This type of device replaces the classic viscous dashpot found in traditional tuned mass dampers (TMDs) for a friction damper. It has been shown that FTMDs can enhance the performance of traditional TMDs (Etedali *et al*. 2019, Jiang *et al*. 2019).

Furthermore, many seismic isolation systems for buildings and bridges are friction-based devices (Ozbulut and Silwal 2016, Shahbazi and Taghikhany 2017 and Calvi and Calvi 2018).

Numerous forms of friction can effectively be used to mitigate structural damage. This paper focuses entirely on Coulomb sliding friction, where irrecoverable work is carried out by the tangential force required to slide one body across the surface of another.

The main purpose of this paper is to find friction coefficients that maximize energy dissipation for different near-fault seismic records. In order to do this, different contacting interfaces were considered and tested so as to determine their friction ratios. Furthermore, relationships between friction coefficients and earthquake record's parameters such as peak ground acceleration (PGA) and root mean square (RMS) acceleration were evaluated.

2. Theoretical background

Simple systems with Coulomb friction have been studied for a long time. In this sense, Den Hartog (1931) studied a SDOF system excited by a harmonic force. He was able to show both analytically and experimentally that,

*Corresponding author, Ph.D., Professor,
E-mail: dambrosini@uncu.edu.ar
[a] M.Sc., Ph.D. Student
[b] Ph.D., Professor

ISSN: 1738-1584 (Print), 1738-1991 (Online)

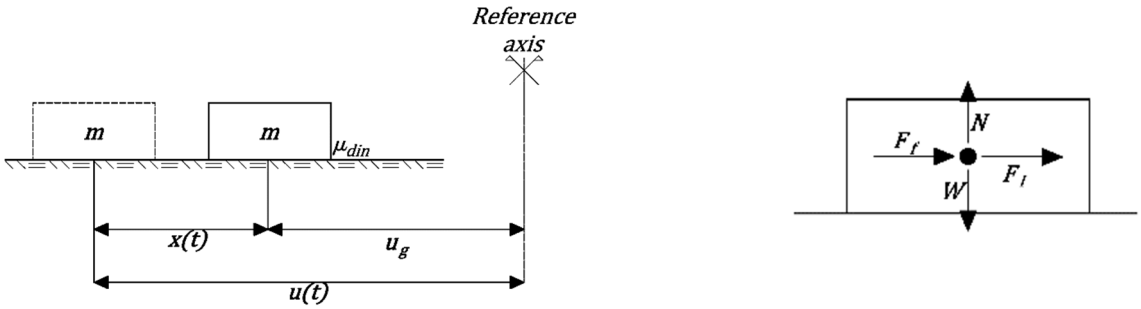

(a) Block's initial position (solid line) and position at time interval t_i (dashed line) (b) Forces acting on the block

Fig. 1 SDOF friction problem formulation

depending on system's properties, the mass may constantly slip or it may stop sliding during parts of each cycle. This last study was particularly important as it was able to unveil the motion's stick-slip nature. Later, Hundal (1979) deduced closed-form analytical equations for a SDOF system with friction force acting between mass and ground. This type of model is also currently used to simulate the mechanical response of the sliding bearings in seismic isolation systems (Ozbulut and Silwal 2016).

In order to understand the different aspects involved in energy dissipation by means of friction, a brief summary of the kinematic equations that govern a block sliding on a friction surface is needed. López *et al*. (2004) thoroughly discuss this subject in their study.

2.1 Problem formulation

Consider a rigid block with mass m resting on a flat horizontal surface. The dynamic friction ratio μ in the contact interface is supposed to remain constant and equal to the static friction coefficient throughout this paper. The problem consists in finding the block's response corresponding to an arbitrary excitation of the supporting surface represented by base acceleration $\ddot{u}_g(t)$.

Fig. 1(a) shows an illustration of the block in its initial position (full line) and the block's position at interval t_i (dashed line). The block's absolute position $u(t)$ is measured from a fixed reference axis, while the block's relative position $x(t)$ is measured form the block's original position. Additionally, $u_g(t)$ represents the absolute base displacement measured from the reference axis.

The normal force perpendicular to the contact surface is denoted by $\mathcal{N}$. Note that in the case of a horizontal surface, this force equals the block's dead weight $\mathcal{W} = m\,g$, where g is the gravity acceleration. If the contact surface is horizontal, both friction forces (F_f) and inertial forces (F_I) act horizontally, but they may be opposed to one another depending on the block's relative velocity ($\dot{x}$). Fig. 1(b) illustrates all the forces acting on the block.

Assuming the block can be represented as a particle, its equation of motion is expressed as follows

$$m \cdot \ddot{x} + \text{sgn}(\dot{x}) \cdot \mu \cdot \mathcal{N} = -m \cdot \ddot{u}_g \tag{1}$$

Eq. (1) is a second order nonlinear differential equation. The nonlinearity appears because the friction force term depends on the sign function of the block's relative velocity. This is

$$F_f = \text{sgn}(\dot{x}) \cdot \mu \cdot \mathcal{N} = \begin{cases} \mu \cdot \mathcal{N} & if\ \dot{x}(t) > 0 \\ 0 & if\ \dot{x}(t) = 0 \\ -\mu \cdot \mathcal{N} & if\ \dot{x}(t) < 0 \end{cases} \tag{2}$$

2.2 Stick-slip motion

The block can experience two different types of movement when subjected to an arbitrary base excitation.

On one hand, the block can move alongside with the base. In this case, relative displacements between base and block are null. The mathematical condition for this type of motion, called stick, is that the block's absolute velocity equals the base's absolute velocity, that is $\dot{u}(t) = \dot{u}_g(t)$.

On the other hand, the block can slide and move independently of the base. For this type of motion, known as slip, relative displacements vary depending on time. The mathematical condition in this case is that the block's absolute velocity differs from the base's absolute velocity, hence $\dot{u}(t) \neq \dot{u}_g(t)$. Note that under the assumption that dynamic friction ratio remains constant and equal to static friction ratio, it can be verified that the block's sliding acceleration remains constant and equal to a limiting value of $\pm\mu \cdot g$ during the slip phase.

The process that summarizes the block's motion for this problem is as follows: when base excitation begins, the block remains in stick situation moving alongside with the base. This stick phase lasts until the block's absolute acceleration equals the limiting value given by the friction force. Once this limit is surpassed, the block begins to slip and move independently from the base. The end of the slip phase occurs when the block's absolute velocity equals the absolute velocity of the base. After that, stick phase restarts.

2.2.1 Harmonic base excitation

In the particular case of harmonic base excitation, a normalized friction force parameter (f_f) was defined in order to identify whether the phase of the movement is stick or slip (López *et al*. 2004)

$$f_f = \pm \frac{F_f}{m \cdot u_{g0} \cdot (2 \cdot \pi \cdot f_0)^2} \tag{3}$$

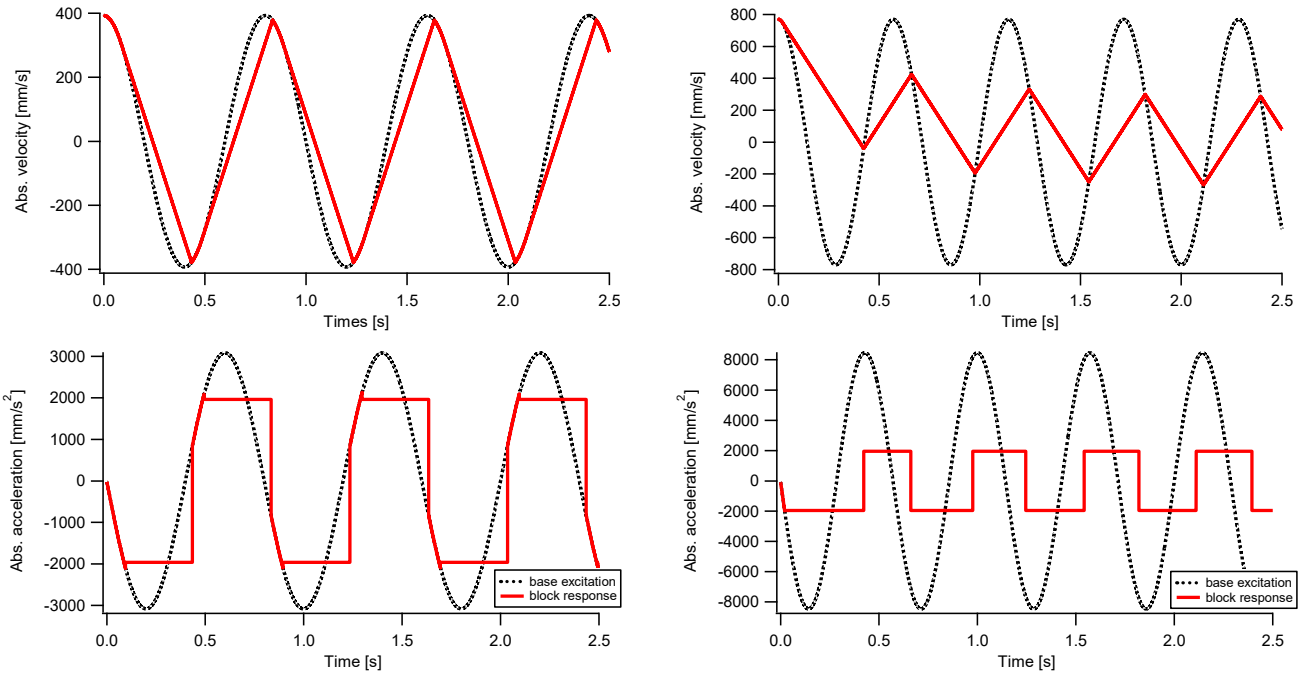

(a) Stick-slip motion, $f_f = 0.636$ (b) Block continuously slipping, $f_f = 0.232$

Fig. 2 Absolute velocity (top) and absolute acceleration (bottom) of block and base

Where:

f_0: base excitation frequency.

u_{g0}: base displacement amplitude for harmonic excitation.

In Eq. (3), positive or negative sign corresponds to negative or positive base acceleration, respectively.

If $|f_f| \geq 1$, the block does not experience slip and it continuously moves with the same displacement, velocity and acceleration as the base.

On the other hand, if $|f_f| < 1$, the block will unfailingly slip at some time. There are two alternatives in this case: they can be recognized by introducing a threshold value of the normalized friction force parameter. It can be probed that the value of this threshold remains constant (López *et al*. 2004).

$$f_{f\ threshold} = \sqrt{\frac{1}{1+\frac{\pi^2}{4}}} \approx 0.5370 \tag{4}$$

Furthermore, if the normalized friction force parameter is below this limiting value, the block will permanently slide on the base. Conversely, if the normalized friction parameter is larger than $f_{f\ threshold}$ but smaller than 1, the block will alternate between stick and slip phases.

Fig. 2 shows two typical type of responses for harmonic base excitation. Fig. 2(a) depicts the case when $f_{f\ threshold} < |f_f| < 1$which corresponds to stick-slip motion. Firstly, the block moves alongside with the base (stick). This is clear from the graphs, as the block's response curves match exactly base's excitation records. Then, when the block's absolute acceleration exceeds the limit of approximately 2000 mm/s^2, set for this particular example, slippage occurs and the block begins to slide. Note that the block's response during this phase is characterized by constant acceleration and linear velocity. Slip continues until the moment when the block's velocity equals that of the base, then the stick phase begins again. It is important to point out that despite these phase changes, the block's motion is still periodic, as probed by López *et al*. (2004).

The case when $|f_f| < f_{f\ threshold}$ is illustrated in Fig. 2(b). When the base starts moving, the block's response parameters are equal to that of the base, indicating the initial stick phase. Nevertheless, once the limiting acceleration value is surpassed, the block starts slipping with constant acceleration and linear velocity. Moreover, for this type of motion the block never returns to a stick phase. The moment when block and base's velocity become equal, a sudden change in the block's absolute acceleration sign takes place, but its magnitude still remains equal to that of the limiting value where sliding onsets.

Energy dissipation was also studied for harmonic excitation. In that sense, López *et al*. (2004) analyzed the relationship between the normalized friction force parameter and dissipated energy per cycle. They were able to probe that maximum energy dissipation occurs when the block is permanently slipping and for a constant value of f_f, that is

$$f_{f\ max} = \frac{\sqrt{2}}{\pi} \approx 0.4502 \tag{5}$$

Using this value, it is possible to determine the friction ratio (μ_{max}) that maximizes energy dissipation by combining Eqs. (3) and (5).

$$\mu_{max} = \frac{f_{f\ max} \cdot u_{g0} \cdot (2 \cdot \pi \cdot f_0)^2}{g} \tag{6}$$

Additionally, it is important to point out that the maximum achievable value of dissipated energy for harmonic excitation depends on the block's mass, the displacement amplitude and frequency excitation of the base.

2.2.2 Arbitrary base excitation

The problem becomes more complex for an arbitrary base excitation. This type of excitation can be represented by a seismic record which contains not one but several dominant frequencies. As a consequence, a numerical solution for the problem is proposed.

The time integration scheme for Eq. (1) described in this section is based on the Newmark-beta method with coefficients $\gamma = 1/2$ and $\beta = 1/4$. This means that acceleration remains constant during the integration interval.

Total analysis time is subdivided in intervals with a duration of Δt. As hypothesis, the values of the block's response for time instant t_i are known. These response values are indicated as

$$\begin{aligned} x(t_i) &= x_i \\ \dot{x}(t_i) &= \dot{x}_i \\ \ddot{x}(t_i) &= \ddot{x}_i \end{aligned} \tag{7}$$

The block's response parameters for interval $t_{i+1} = t_i + \Delta t$ (x_{i+1}, $\dot{x}_{i+1}$ and $\ddot{x}_{i+1}$) are calculated based on the known response parameters for instant t_i.

Discrete Newmark-beta method expressions for relative velocity and acceleration are as follows

$$\ddot{x}_{i+1} = \frac{4}{\Delta t^2} \cdot (x_{i+1} - x_i) - \frac{4}{\Delta t} \cdot \dot{x}_i - \ddot{x}_i \tag{8}$$

$$\dot{x}_{i+1} = \frac{2}{\Delta t} \cdot (x_{i+1} - x_i) - \dot{x}_i \tag{9}$$

Eq. (1) must hold true for time instant t_{i+1}, this means that

$$m \cdot \ddot{x}_{i+1} + m \cdot \ddot{u}_{g\,i+1} + \operatorname{sgn}(\dot{x}_{i+1}) \cdot \mu \cdot \mathcal{N} = 0 \tag{10}$$

If integration step Δt is sufficiently small, then it is possible to assume that $\operatorname{sgn}(\dot{x}_{i+1}) = \operatorname{sgn}(\dot{x}_i)$. As a result

$$m \cdot \ddot{x}_{i+1} + m \cdot \ddot{u}_{g\,i+1} + \operatorname{sgn}(\dot{x}_i) \cdot \mu \cdot \mathcal{N} = 0 \tag{11}$$

Considering the expression for $\ddot{x}_{i+1}$ given in Eq. (8), replacing it in Eq. (11) and solving for x_{i+1}

$$\begin{aligned} x_{i+1} = x_i + (\Delta t \cdot \dot{x}_i) + \left(\frac{\Delta t^2}{4}\right) \cdot \ddot{x}_i - \left(\frac{\Delta t^2}{4}\right) \cdot \ddot{u}_{g\,i+1} \\ -\operatorname{sgn}(\dot{x}_i) \cdot \frac{\Delta t^2}{4 \cdot m} \cdot \mu \cdot \mathcal{N} \end{aligned} \tag{12}$$

Once x_{i+1} is determined, $\ddot{x}_{i+1}$ and $\dot{x}_{i+1}$ can be computed by using Eq. (8) and Eq. (9), respectively. After that, one can proceed to the following time interval.

Algorithm for arbitrary base excitation

In order to apply the expressions mentioned above, a few auxiliary variables need to be introduced. Firstly, a phase indicator U is defined. If $U = 0$ for the analyzed time interval, the block is in stick situation. Contrarily, if $U = 1$, then the block is in the slip phase. Secondly, acceleration and velocity tolerance values need to be entered.

An algorithm for integrating Eq. (1) using the Newmark-beta method is described below. Notice that this particular algorithm requires the complete base excitation time-history, including velocities and displacements, to be known. In this sense, both displacement and velocities can be obtained by integrating base acceleration data with the method described by Yang *et al*. (2006).

Fig. 3 illustrates the block's absolute time-history response when the base is subjected to an earthquake record [Mendoza 1985]. These results were obtained using the algorithm described above with a constant friction ratio of 0.10. Acceleration tolerance was set at 1.10^{-5} times the value of the PGA, while the velocity tolerance was adopted as 1.10^{-2} the value of the peak ground velocity (PGV). These tolerance values yielded good results when working with earthquake records as base excitation.

Unlike harmonic base excitation where the block can slide permanently depending on the value of parameter f_f, for seismic base excitation the type of motion is mostly stick-slip. This result was experimentally verified for short duration seismic records with PGA values smaller or equal to $0.40g$ and relatively low friction coefficients ($\mu \leq 0.20$), and it will be thoroughly discussed in the section referring to experimental studies.

The nature of the stick-slip motion can clearly be seen both in the absolute velocity and acceleration plots of Fig. 3. In the latter, slipping onsets several occasions when acceleration becomes approximately constant at a value of around 1000 mm/s^2. The rest of the time the block remains in stick state, with the block's acceleration reproducing exactly that of the base.

During intervals where slipping occurs, the block's absolute velocity becomes linear and it does not match base excitation. However, when the block moves alongside with the base, the two curves match perfectly.

The block's absolute displacement history shows instants when its curve becomes parallel to the curve that represents base excitation. These time intervals correspond to stick phases.

2.2.3 Energy dissipation

In this paper energy balance is assessed using the absolute input energy approach described by Uang and Bertero (1990).

Energy balance can be deduced by integrating Eq. (1). For this particular problem three different types of energy are recognized: kinetic energy ($E_{k\,abs}$), energy dissipated by friction ($E_{d\,f}$) and absolute energy input ($E_{I\,abs}$).

$$E_{k\,abs} + E_{d\,f} = E_{I\,abs} \tag{13}$$

Algorithm 1 Block response for arbitrary base excitation

INPUT

Base excitation record $\{\boldsymbol{u_g}, \boldsymbol{\dot{u}_g}, \boldsymbol{\ddot{u}_g}\}$
Block's mass m
Friction ratio μ
Time integration step Δt
Acceleration tolerance a_t
Velocity tolerance v_t

INITIALIZATION

Read final time t_f from base excitation records
Compute limiting ground acceleration beyond which slipping occurs $\ddot{u}_{lim}$

$$\ddot{u}_{lim} = \mu \cdot g$$

Initialize step counter and time $i = 0,\ t_i = 0$.
Initialize block's relative response vectors $\{\boldsymbol{x}, \boldsymbol{\dot{x}}, \boldsymbol{\ddot{x}}\}$
Initialize block's absolute response vectors $\{\boldsymbol{u}, \boldsymbol{\dot{u}}, \boldsymbol{\ddot{u}}\}$
Initialize $U_i = 0$.
Calculate initial relative acceleration, for resting state $x_i = 0$ and $\dot{x}_i = 0$

$$\ddot{x}_i = -\ddot{u}_{g\,i} - \text{sgn}(\dot{x}_i) \cdot \frac{\mu \cdot \mathcal{N}}{m}$$

Compute block's starting absolute response

$$u_i = u_{g\,i} + x_i$$
$$\dot{u}_i = \dot{u}_{g\,i} + \dot{x}_i$$
$$\ddot{u}_i = \ddot{u}_{g\,i} + \ddot{x}_i$$

Update $t_{i+1} = t_i + \Delta t$

LOOP OVER TIME INCREMENTS

Do while $t_{i+1} < t_f$

Update relative displacement and velocity with Eq. (12) and Eq. (9), respectively.

If $U_i = 0$, then:

If $|\ddot{u}_{g\,i+1}| - \ddot{u}_{lim} < a_t$ → stick phase

$$U_{i+1} = 0$$
$$\ddot{x}_{i+1} = 0$$

Else → change from stick to slip phase

$$U_{i+1} = 1$$
$$\ddot{x}_{i+1} = 0$$

End if

Else ($U_i = 1$ block sliding in previous step)

If $|\dot{x}_i| > v_t$ → block continues sliding

$$U_{i+1} = 1$$
$$\ddot{x}_{i+1} = \frac{4}{\Delta t^2} \cdot (x_{i+1} - x_i) - \frac{4}{\Delta t} \cdot \dot{x}_i - \ddot{x}_i$$

Else → block sticks to the base

$$U_{i+1} = 0$$
$$\ddot{x}_{i+1} = 0$$

End if

End if

Update block's absolute response

$$u_{i+1} = u_{g\,i+1} + x_{i+1}$$
$$\dot{u}_{i+1} = \dot{u}_{g\,i+1} + \dot{x}_{i+1}$$
$$\ddot{u}_{i+1} = \ddot{u}_{g\,i+1} + \ddot{x}_{i+1}$$

Update time increment

$$i = i + 1$$
$$t_{i+1} = t_i + \Delta t$$

End do

EXIT

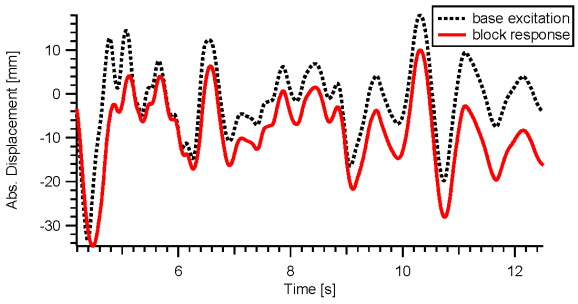

(a) Abs. displacement v. Time.

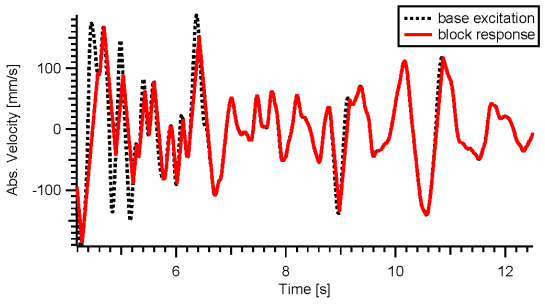

(b) Abs. velocity v. Time

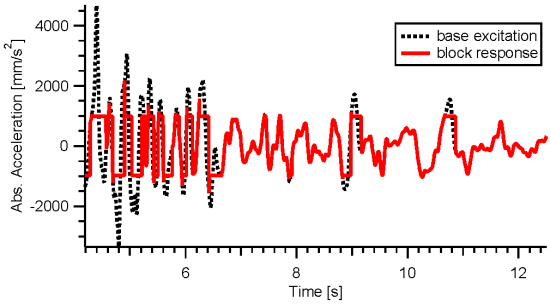

(c) Abs. acceleration v. Time

Fig. 3 Absolute time history response $\mu = 0.10$, $\Delta t = 0.003\ s$, Mendoza record

Where

$$E_{k\,abs} = \frac{1}{2} \cdot m \cdot \dot{u} \tag{14}$$

$$E_{d\,f} = \int F_f \cdot dx \tag{15}$$

$$E_{I\,abs} = \int m \cdot \ddot{u} \cdot du_g \tag{16}$$

Discrete energy balance

Even though Eqs. (14), (15) and (16) provide concise mathematical definitions for the types of energy involved in the problem, they are of limited applicability when working with earthquake records where discrete expressions to calculate the value of each type of energy for the different time steps are more useful.

Absolute kinetic energy can be directly evaluated as a function of the block's absolute velocity in the same time step. Hence for time instant t_{i+1}

$$E_{K\,abs\,i+1} = \frac{1}{2} \cdot m \cdot \dot{u}_{i+1} \tag{17}$$

The increment of energy dissipated by friction for instant t_{i+1} can be computed as

$$\begin{aligned} \Delta E_{d\,f\,i+1} &= F_{f\,i+1} \cdot \dot{x}_{i+1} \cdot \Delta t \\ &= -m\ddot{u}_{i+1} \cdot \left(\dot{u}_{i+1} - \dot{u}_{g\,i+1}\right) \cdot \Delta t \end{aligned} \tag{18}$$

Based on Eq. (15), energy dissipated by friction should be numerically integrated over time. Thus

$$E_{d\,f\,i+1} = E_{d\,f\,i} + \Delta E_{d\,f\,i+1} \tag{19}$$

In addition, the incremental value of absolute external energy supplied to the block can be expressed as follows

$$\Delta E_{I\,abs\,i+1} = m \cdot \ddot{u}_{i+1} \cdot \dot{u}_{g\,i+1} \cdot \Delta t \tag{20}$$

Therefore, the absolute external energy for time interval t_{i+1} yields

$$E_{I\,abs\,i+1} = E_{I\,abs\,i} + \Delta E_{I\,abs\,i+1} \tag{21}$$

3. Single channel experimental tests

Experimental studies were carried out with the purpose of evaluating energy dissipation capacity of blocks sliding on a flat surface. These dynamic tests were performed on a shacking table at Universidad Nacional de Cuyo's Experimental Dynamics Laboratory.

3.1 Test setup

The shaking table consists of a MOOG 6DOF2000E motion platform mounted on the laboratory's reactive slab. This platform has six hydraulic jacks positioned in different directions. Such a configuration allows the system to reproduce base excitations with up to 6 DOF. The table's maximum payload is $10\,kN$. Acceleration, velocity and displacements limits are $0.60\,g$, $0.50\,m/s$ and $0.25\,m$, respectively. The direction of base excitation in the tests described in this paper was parallel to the aluminum channel's longitudinal direction.

Test setup as well as instrumentation are illustrated in Fig. 4. The test basically consisted of a lead block contained by a U-shaped aluminum channel type section with the open end facing upwards. This setup allowed the block to slide freely when the shaking table moved. Five different types of contact interfaces between block and aluminum channel were considered for the test series. To materialize them, individual coatings layers were bonded to the block and channel.

The aluminum section was fixed to the shaking table's platform using two bolts, one on each end. This fixed condition made it possible to assume that channel's accelerations are equal to that of the shaking table.

The aluminum channel section was made up from an AA6063 alloy with T6 tempering process. Cross section's dimensions were: 90 mm of outside depth, 40 mm of outside flange width and a uniform thickness of 5 mm for flanges and web.

Lead block dimensions are indicated in Fig. 5(a). They

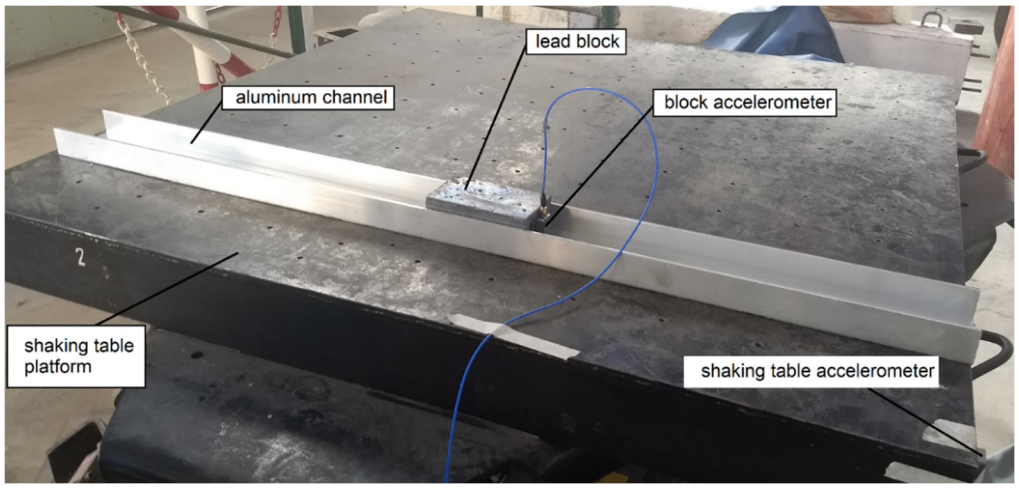

Fig. 4 Dynamic test setup

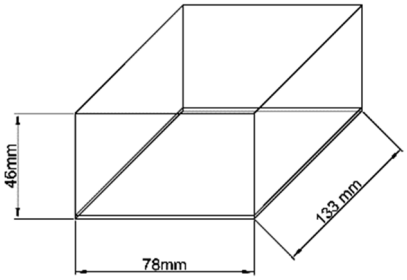

(a) Block's dimensions

(b) PTFE sheet attached to block's bottom face

Fig. 5 Lead blocks used for dynamic tests

were adopted so that the block's total mass was approximately equal to 5.10 kg. In addition, the block was shaped so that it fitted almost perfectly on the channel, with flanges impeding block's out-of-axis motion.

Note that the dimensions in Fig. 5(a) include 1.5 mm of Teflon (polytetrafluoroethylene, PTFE) sheet thickness attached to the bottom of the block. Epoxy adhesive was used to bond the sheet to the block's bottom face. The block's bottom face and the PTFE sheet can be seen in Fig. 5(b).

3.2 Instrumentation

Two accelerometers were used in these tests: one to register the block's acceleration and the other to measure shaking table's acceleration. The position of both of these transducers is showed in Fig. 4. It is important to point out that they were both placed so as to register the longitudinal components of the acceleration in the motion direction. Capacitive accelerometers PCB Piezotronics 3701D1FA3G were employed, with a sensitivity of 700 mV/g and a measuring range of ±3 g. The accelerometers were connected to signal conditioners PCB Piezotronics 478A01. The signal was digitized by a data acquisition board Computerboards PC-CARD-DAS16/16 of 100 kHz and HP VEE 6.0 software was employed to record the time history response.

Additionally, after the end of each test the block's residual displacement was measured. These measurements took place immediately after the block stopped moving.

The sampling rate adopted for these tests was of 500 samples per second. This is equivalent to a time interval of 0.002 s between measurements. Note that according to the Nyquist-Shannon sampling theorem, this allows to recognize frequencies of up to 250 Hz in the waveforms.

3.3 Test protocol and base excitation records

Both harmonic and earthquake records were selected as input signals for the shaking table. These records were entered in the system using control software. At this stage they were converted from digital to analog signals. Then, after being properly conditioned, these signals were sent to the servo valves that operate the motion platform's hydraulic jacks. These jacks have the function of reproducing the ground's motion.

For the harmonic records, two different displacement amplitudes (u_{g0}) were considered: 30 and 5 mm. For the former amplitude value, two different excitation frequencies were considered: 1 and 2 Hz. While for the latter, only a 3 Hz frequency was considered.

Two different seismic records were selected for the tests: the KJMA station Kobe record (comp. 090), and the Mendoza [1985] record. Note that the first record was downscaled by a factor of 0.65 so that its PGA did not exceed the shacking table's acceleration limit. The Kobe record was chosen to characterize an ultimate limit state demand, while the Mendoza record exemplifies a serviceability limit state demand. Both records are of the near-fault type.

3.4 Contact interfaces

As seen in Eq. (18), energy dissipated by friction depends both on friction force as well as the block's relative velocity to the metallic frame. It has been stated before that for earthquake record base excitation it is not possible for the block to continuously slide. An alternative consists in reducing the friction ratio of the contact interface so that the block can slip during a larger period of time. However, this reduction also induces a decline of the friction force and, consequently, energy dissipation.

Different types of contact interfaces with varying friction ratios were tested in order to achieve maximum energy dissipation. The PTFE sheet shown in Fig. 5(b) was glued to the block's bottom face for all the interfaces studied.

Materials and different superficial treatments applied to the contact surface are specified in Table 1.

In the case of interface I, the block slides over the channel's aluminum surface, which was previously cleaned and treated with penetrating oils.

The silicone oil used in interfaces III and V is made from dimethyl siloxane and finished trimethylsiloxy. Its cinematic viscosity is equal to 350 cSt at 25°C.

On the other hand, the commercial lubricant used in interfaces IV and V is a mixture of petroleum by-products with added PTFE particles.

3.5 Results

Results of the dynamics tests are discussed in this section. Special attention is paid to the block's measured acceleration records as well as to the friction coefficients for each tested interface.

3.5.1 Interface I

With this contact interface it was possible to achieve continuous slipping for some harmonic base excitation records.

One of those cases is shown in Fig. 6 where both shaking table and block's acceleration are displayed as a function of time. The difference between these two records is quite noticeable. It is clear that the block was able to slide steadily. From the graph it becomes evident that block's acceleration presents a limiting value, both positive and negative, which cannot be exceeded. This limiting value represents the block's almost constant acceleration when it enters the slip phase. Looking at the first 1.00 to 1.50 s of the record, it is possible to notice that block's absolute accelerations match almost exactly the accelerations of the shaking table, therefore indicating an expected stick phase at the start of the motion.

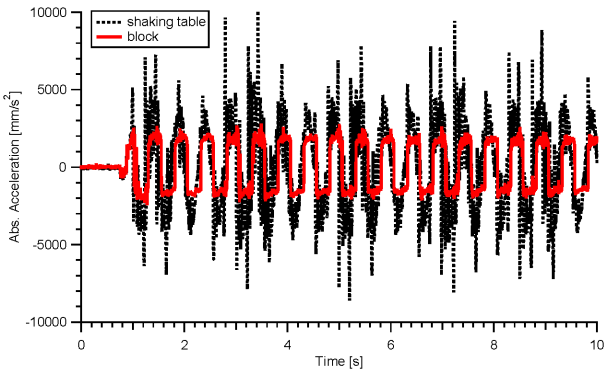

Fig. 6 Test results interface I $u_{g0} = 30\ mm$ and $f_0 = 2\ Hz$

Fig. 7 PTFE sheet bonded to aluminum channel

It is also relevant to point out that for this interface it was possible to achieve friction ratios between 0.18 and 0.22. These values were computed using the block's limiting acceleration values when in slip phase, which according to the plot in Fig. 6 were approximately of 2000 mm/s^2.

3.5.2 Interface II

In order to materialize this interface a PTFE sheet was glued to the aluminum channel's horizontal face. This is illustrated in Fig. 7. This interface evidenced lower friction ratios and, once more, it was possible to achieve continuous slipping for some harmonic records.

The block's response was clearly distinguishable from base excitation for the harmonic records. Furthermore, block's absolute acceleration exhibits the pulse-like behavior previously discussed.

Fig. 8 presents the test results for the Kobe acceleration record. It is possible to observe that in this case sliding was not continuous. Two main slipping time intervals can be noticed: approximately from 7.00 to 10.00 s and from 11.00 to 14.00 s. Coincidentally, base record's acceleration peaks occur during these time intervals. After this test the block experienced a residual displacement of 95 mm with respect to its original position. This displacement was the largest of the whole test series.

Measured friction ratios for this interface were approximately between 0.09 and 0.12. These values are lower than the ones determined for interface I, hence slipping periods tend to be a little longer.

3.5.3 Interface III and interface V

For the cases of interface III and interface V surface treatment included silicon oil. In the case of interface III,

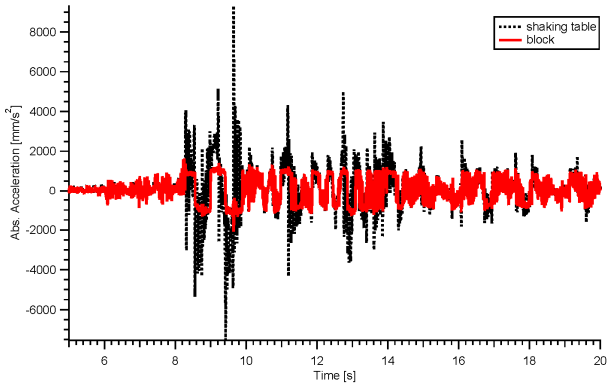

Fig. 8 Test results interface II Kobe record

Table 1 Contact interfaces considered for the tests

Interface	Channel face	Block face	Surface treatment
I	Clean aluminum	PTFE	Commercial lubricant with penetrating oils
II	PTFE	PTFE	None
III	PTFE	PTFE	Silicon oil
IV	PTFE	PTFE	Commercial lubricant with penetrating oils and added PTFE
V	PTFE	PTFE	Commercial lubricant with penetrating oils and added PTFE, and silicon oil

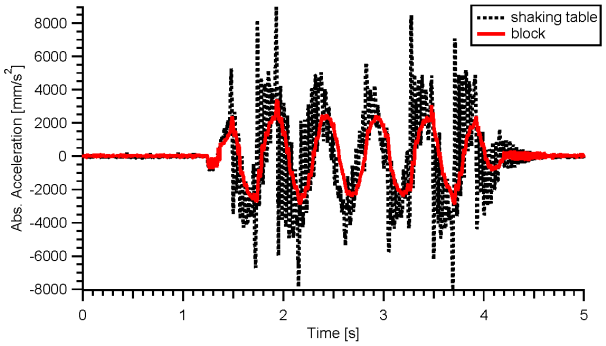

Fig. 9 Test results interface V
$u_{g0} = 30\ mm$ and $f_0 = 2\ Hz$

where PTFE-PTFE contact surfaces were treated exclusively with silicon oil, results were not satisfactory as it was not possible to achieve the pulse-like behavior that characterizes block's slipping.

Despite being able to visibly notice block sliding in these tests, it was not as evident as for the others contact surfaces. This was attributed to the fact that the oil formed a thin layer with shear resistance between the two contacting surfaces, therefore making it harder for the block to slide. Such resistance was provided by the silicon's viscosity.

As showed in Table 1, interface V consists of the two PTFE surfaces treated with both silicon oil and a lubricant oil with added PTFE. The test results for this surface were also not satisfactory as the silicon oil's viscous effect prevailed over other factors.

The effect just mentioned can clearly be seen in Fig. 9

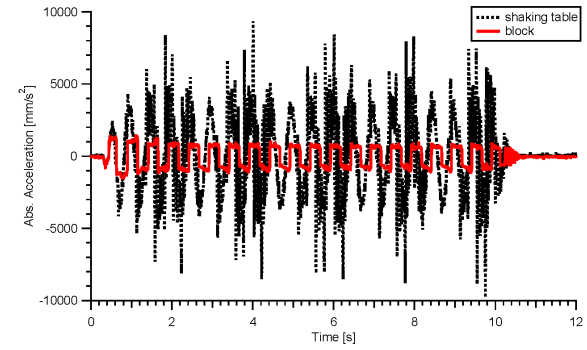

(a) Harmonic record with $u_{g0} = 30\ mm$ and $f_0 = 2\ Hz$

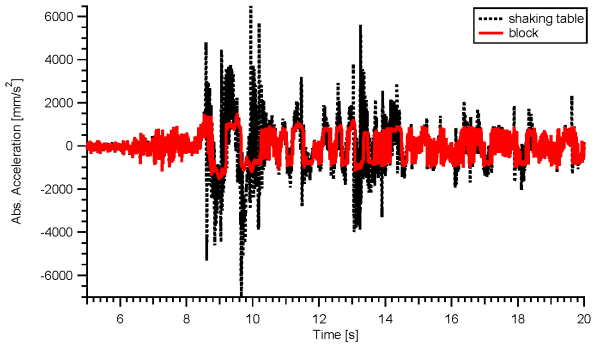

(b) Kobe record

Fig. 10 Test results interface IV

where a strong resemblance between block and base's accelerations can be noticed. In addition, a high-frequency filter effect can be observed in the block's record when compared to the base record.

3.5.4 Interface IV

In the case of interface IV surface treatment consisted of a commercial lubricant with penetrating oils and added PTFE.

The recorded block response to an harmonic excitation with $u_{g0} = 30\ mm$ and $f_0 = 2\ Hz$ is displayed in Fig. 10(a). From the graph, differences between block and base excitation become evident. Almost constant pulse-like behavior is observed for the block's acceleration, this means constant sliding. Additionally, it is possible to notice that block's slipping acceleration slightly decreases in the first few cycles. This takes place until it reaches an almost constant value of $\pm 0.08\ g$ for the higher cycles.

Results obtained for the Kobe record are shown in Fig. 10(b). In this case, as for the harmonic records, block's slipping acceleration tends to decrease as the number of slipping cycles increases. The absolute acceleration for the first slipping phase was approximately $0.12\ g$, but for latter slip phases it varied between $0.10\ g$ and $0.07\ g$. Block sliding was not continuous in this test, nevertheless several slipping phases could be distinguished from the measured block response.

Interface IV exhibited the lowest friction ratios of all the test series. These low values allowed the block to slide not only for the Kobe record, but also for the Mendoza record which presents acceleration values associated with serviceability states. As a counterpart, friction ratios were more variable, especially for the first four or five slipping cycles. This variation was mostly limited between 0.12 and 0.07.

3.5.5 Energy balance

Using the basic concepts presented on section 2.2.3, a basic routine was written in order to compute the values of different energy types for the dynamic test's records. Note that these records were integrated over time when necessary.

For the analysis exhibited here the cumulated values of external energy provided to the system as well as energy dissipated by friction were considered. Kinetic energy instant values were used in the graphs.

Special attention was given to the values computed for interfaces II and IV, as they were later used for the calibration of computational models.

In Figs. 11(a), (b) and (c) energy values computed for three different dynamic tests using friction interface II were plotted. It is important to remark that friction dissipation was larger for the base excitation consisting of harmonic displacements. This result was reasonable, as in this case the block was able to continuously slide.

The observations made for contact interface II are also applicable to interface IV. The energy values obtained for the tests are plotted in Figs. 12(a), (b) and (c) for the harmonic, Mendoza and Kobe records, respectively. Moreover, energy values computed for these cases were very similar to the ones obtained for the tests carried out

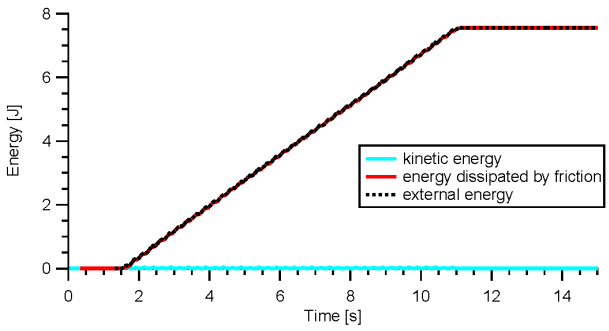

(a) Harmonic record with $u_{g0} = 30\ mm$ and $f_0 = 2\ Hz$

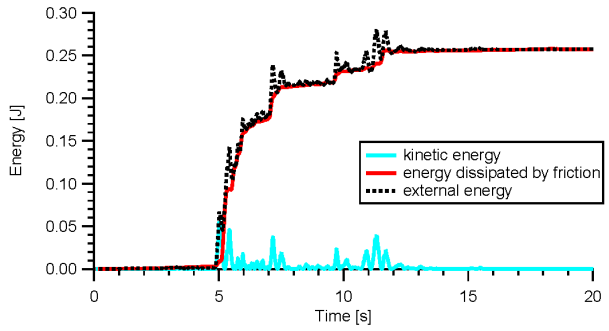

(b) Mendoza record

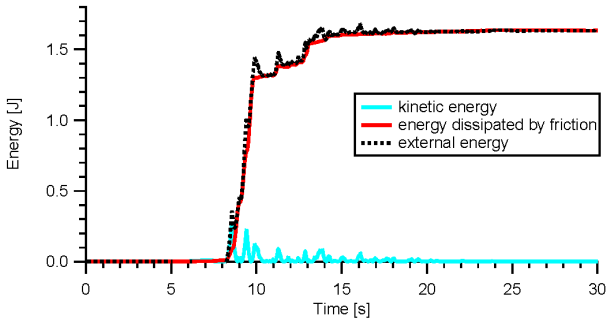

(c) Kobe record

Fig. 11 Different types of energy for dynamic tests, interface II

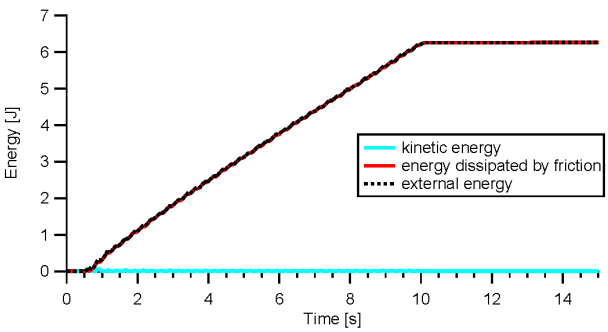

(a) Harmonic record with $u_{g0} = 30\ mm$ and $f_0 = 2\ Hz$

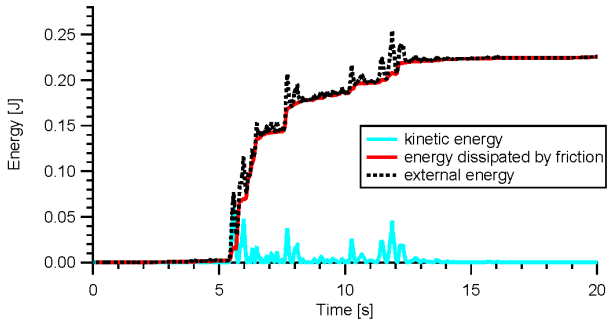

(b) Mendoza record

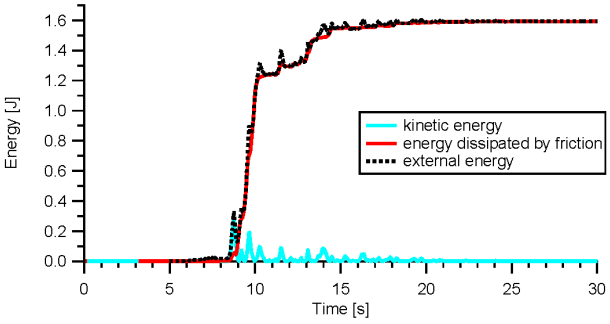

(c) Kobe record

Fig. 12 Different types of energy for dynamic tests, interface IV

with interface II.

4. Computational models

Test results discussed in section 3 for both interface II and IV were used to calibrate parameters for computational models built in ANSYS software (ANSYS 2010). These models were calibrated and later used for the energy dissipation maximization study.

4.1 Model description

Models basically consisted of two distinct solid bodies: on one hand, the channel base and, on the other, the lead block. The base is made up of an 80 mm width and 5 mm thick aluminum sheet. The block dimensions are the same as specified in Fig. 5(a). Its mass was of 5.10 kg. Note that models did not consider the channel's lateral flanges, as it was evident from test results that they did not influence the block's behavior for base excitations applied in the longitudinal direction of the aluminum channel. Fig. 13 shows the model.

Materials unit weight is specified in Table 2.

Regarding boundary conditions, shaking table excitation was represented as remote displacements records applied in a point on the edge of the channel. Additionally, elements self-weight was considered acting in the Y axis direction (Fig. 13).

Both bodies were considered rigid, that is the reason why no meshing was required. The problem was solved using ANSYS Rigid Dynamics module. To define the interaction between bodies two translational joint elements were used: one connects the ground to the channel's base, while the other relates the aluminum base to the block. The first element had all of its degrees of freedom restrained with the exception of displacements in the Z axis direction (Fig. 13). Similarly, the second joint element had the same five degrees of freedom restrained, with displacements in the Z direction allowed but with the distinctive feature that

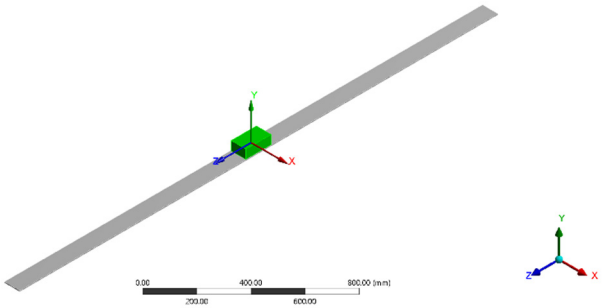

Fig. 13 ANSYS model perspective

Table 2 Model's materials unit weight

Property	Aluminum	Lead
Unit weight [kN/m^3]	27	107

a constant 0.10 friction ratio was specified for motion in this direction.

Fifth order Runge-Kutta method with a tolerance value of 1.10^{-8} was used to integrate the equation of motion. For calibration purposes, integration step was adopted at a constant value of 0.002 s, equal to the sampling time step used in the tests.

The displacement records used as input for the models were obtained by integrating twice the shaking table's acceleration records measured in the dynamic tests. This operation was carried out by specifying a third order polynomic baseline correction and imposing null displacements both at the beginning and the end of the displacement record.

4.2 Results

4.2.1 Block response

The computational model described previously were able to adequately reproduce experimental tests. In order to prove it, the results for three typical input records are going to be analyzed in this section: the harmonic record with $u_{g0} = 30\ mm$, $f_0 = 2\ Hz$, the Mendoza record and, finally, the Kobe record.

In Fig. 14 there is a comparison between the block's absolute acceleration measured in the tests (for interface II) and the computed in the model for the three records mentioned above: (a) harmonic, (b) Mendoza and (c) Kobe. From the graphs it becomes clear that computational model reproduce test results with good accuracy.

The same model results were compared to interface IV test measurements; this can be seen in Fig. 15. From these graphs it can be inferred that model results are also applicable to this interface yielding good adjustment.

In consequence, a 0.10 constant friction ratio replicates appropriately the behavior of both contact interfaces. The first sliding cycles for the experimental results shown in Fig. 15 exhibit higher acceleration magnitudes than the ones estimated with the model. This can be partly attributed to static friction which is always larger than dynamic. However, as the test progress differences between sliding accelerations tend to become less pronounced.

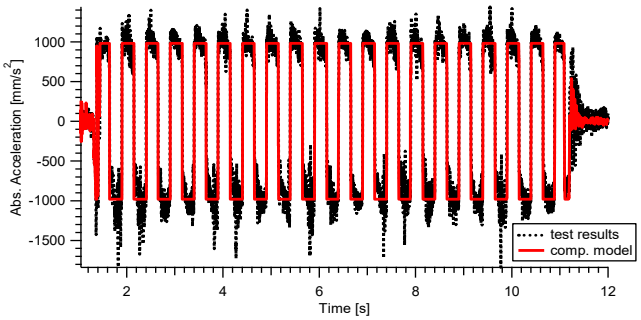

(a) Harmonic record with $u_{g0} = 30\ mm$ and $f_0 = 2\ Hz$

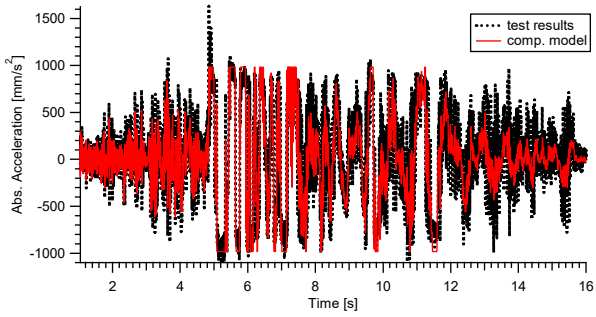

(b) Mendoza record

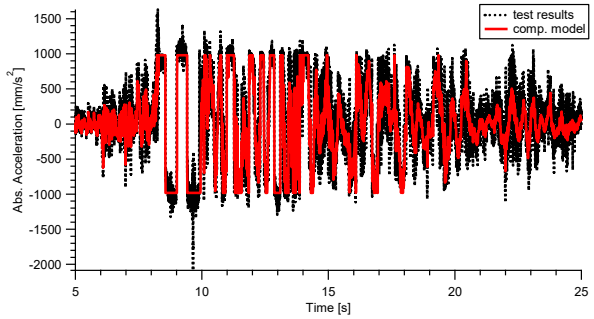

(c) Kobe record

Fig. 14 Block's absolute acceleration experimental (interface II) vs. ANSYS model

Table 3 shows a comparison between residual displacements measured after the tests and the ones obtained with the computational model. It is possible to notice that, for both cases, residual displacements are of the same order of

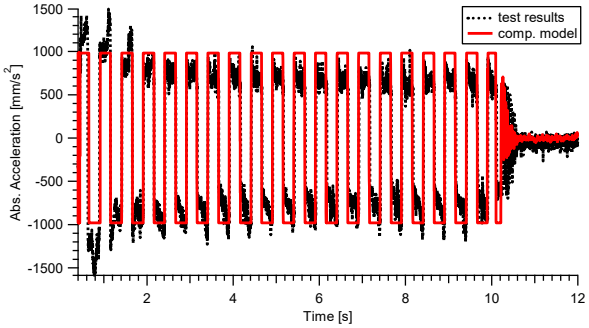

(a) Harmonic record with $u_{g0} = 30\ mm$ and $f_0 = 2\ Hz$

Fig. 15 Block's absolute acceleration experimental (interface IV) vs. ANSYS model

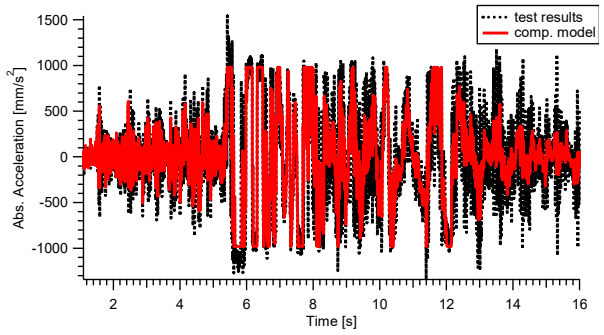

(b) Mendoza record

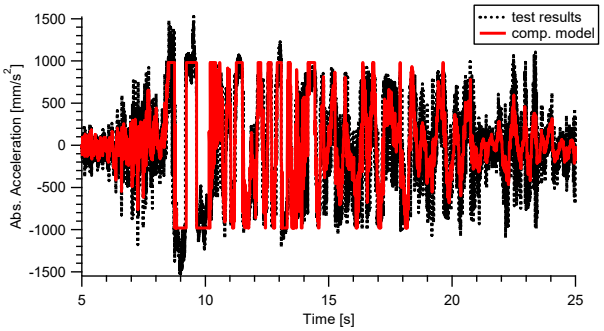

(c) Kobe record

Fig. 15 Continued

Table 3 Residual displacements test vs. comp. models

Interface	Test record	Residual displacements [mm]	
		Test	Model
II	Harmonic	12	23
	Mendoza	18	14
	Kobe	95	124
IV	Harmonic	24	24
	Mendoza	8	11
	Kobe	86	97

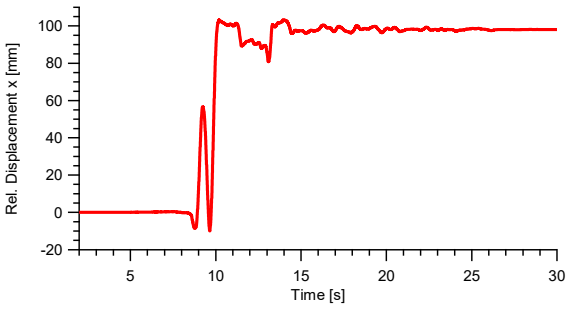

(a) Time v. Block's rel. displacement x

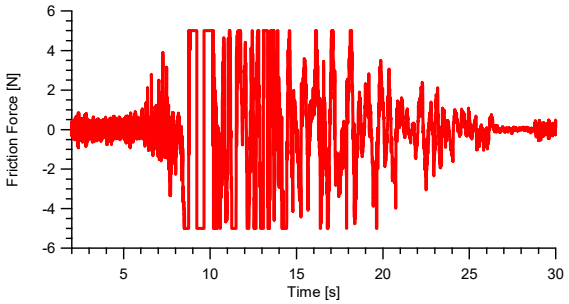

(b) Time v. Friction force

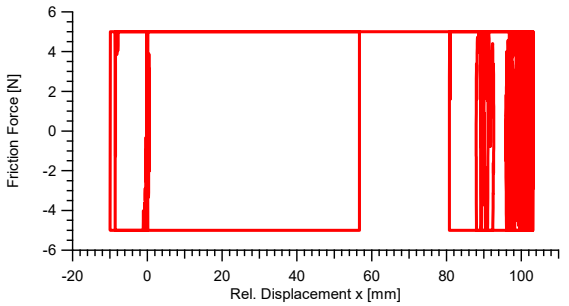

(c) . Block's rel. displacement x v. Friction force

Fig. 16 Computational model response interface IV, Kobe record

magnitude and give a good approximation of those measured in the tests. But it should be observed that the model approximates better the residual displacements obtained in the tests with interface IV.

The variations of the block's relative displacement and friction force with time are shown in Figs. 16(a) and (b), respectively. These results were obtained for a computational model based on a test carried out using the Kobe record. As expected for a friction problem, closed squared hysteresis loops link friction forces to relative displacements, this can be observed in Fig. 16(c). Furthermore, from Fig. 16(a) it is possible to point out the exact periods of time when the block slides, i.e., when relative displacement does not remain constant.

Table 4 summarizes the computed values of energy dissipated by friction for the models. These are compared to the values determined for the complete test series with both interface II and IV. Eq. (19) was used to calculate friction-based dissipated energy.

It is necessary to point out that, in Table 4, all the harmonic records had a displacement amplitude of $u_{g0} = 30\,mm$. While harmonic record 1 and harmonic record 2 had the same motion frequency $f_0 = 2.00\,Hz$, the difference between them was in the total duration of the record which was of 5 s for the former and of 15 s for the latter. On the other hand, both harmonic records 3 and 4 had a frequency of $f_0 = 1.00\,Hz$, with a duration of 5 s for the former and of 15 s for the latter.

From Table 4 it is possible to conclude that computed values of energy dissipated by friction were very similar for both tests and models. Consequently, the models were able to adequately reproduce energy dissipation

In most cases, there is a tendency for the model to slightly overestimate energy dissipated by friction. However, there are exceptions to this trend: with the Harmonics 1 and 2 base excitation records.

Table 4 Comparison between test and model's friction-dissipated energy

Interface	Test record	E_{df} [J]	
		Test	Model
II	Harmonic 1	1.961	1.923
	Harmonic 2	7.557	7.499
	Mendoza	0.273	0.295
	Mendoza	0.258	0.284
	Kobe	1.601	1.754
	Kobe	1.634	1.800
IV	Harmonic 3	0.060	0.078
	Harmonic 4	0.286	0.408
	Harmonic 1	1.997	1.932
	Harmonic 1	1.924	1.918
	Harmonic 2	6.259	7.412
	Mendoza	0.237	0.295
	Mendoza	0.225	0.284
	Kobe	1.593	1.724
	Kobe	1.527	1.698

5. Energy dissipation for different friction ratios

In this section the results of the numerical study carried out to compute energy dissipation for different friction ratios are discussed. For this purpose, different near-fault seismic records were considered. The main objective of this analysis was to identify the friction coefficients for which energy dissipation is maximum.

5.1 Earthquake records

Eight different earthquake records were selected for this analysis. All of these records had short duration, where most of the external energy was supplied in a relatively short period of time. Event's significant duration was computed according to Trifunac and Brady's (1975) criterion, which defines it as the time elapsed between 5 and 95% of the Arias intensity (Arias 1970). This parameter represents an indirect measure of the external energy supplied to a system by the record and it can be calculated as

$$I_A = \frac{\pi}{2g} \cdot \int_0^{t_0} \left[\ddot{u}_g(t)\right]^2 \cdot dt \tag{22}$$

Where:
t_0: Record's total duration.
g: Gravity acceleration.
$\ddot{u}_g$: Ground acceleration.

The main parameters of the selected earthquake records are summarized in Table 5, where M_w represents the event's moment magnitude, t_0 is the record's total duration, t_e is the event's significant duration, Δt_m is the time-sampling interval and PGA is the record's peak ground acceleration. Fig. 17 shows the acceleration time-history of the records, significant duration is highlighted in red.

5.2 Model description

In essence, the numerical models used for this study were the same as the ones presented in section 4.

The analysis was carried out by varying the friction ratio of the translational joint that links the block to the aluminum channel. In this sense, different values were adopted for this ratio: 0.050, 0.075, 0.100, 0.125, 0.150, 0.175 and 0.200. These values were comprised between the ones obtained for interfaces II and IV in the tests.

Mechanical properties of the materials used in the models were the same as the ones specified in Table 2.

Integration method and its tolerance were identical to the ones mentioned in section 4.1.

5.2.1 Effect of time integration step

When studying the effects of different friction ratios on the response, it became evident that, depending on the value of the friction coefficient, time integration step (Δt) can significantly affect the calculated block's acceleration time-history.

Fig. 18 shows computed block's acceleration for $\mu = 0.050$ during Coyote Lake Comp. 230 significant duration using two different time integration steps: $\Delta t = 0.001\ s$ in Fig. 18(a), and $\Delta t = 0.005\ s$ in Fig. 18(b). Notice that there is no apparent difference between both responses.

Table 5 Selected near-fault earthquake records

Event	M_w	Station	Component	t_0 [s]	t_e [s]	Δt_m [s]	I_A [m/s]	PGA [m/s^2]
Cape Mendocino (1992) *	7.01	Petrolia	090	35.96	16.06	0.02	3.82	6.49
Chi Chi (1999) *	7.62	CHY080	N	89.990	22.020	0.005	6.95	8.44
Coyote Lake (1979) *	5.74	Gilroy Array #6	230	27.090	3.210	0.005	0.77	4.14
Coyote Lake (1979) *	5.74	Gilroy Array #6	320	27.100	3.525	0.005	0.68	3.13
Kobe (1995) *	6.90	KJMA	090	149.98	9.52	0.02	5.44	6.18
Mendoza (1985)	6.30	-	-	31.347	8.304	0.003	1.24	4.68
Northridge (1994) *	6.67	Newhall Fire Station	090	39.96	5.86	0.02	4.36	5.72
Parkfield (2004) *	6.00	Cholame 2WA	360	21.065	6.130	0.005	1.11	3.66

*Source: PEER Ground Motion Database (http://peer.berkeley.edu)

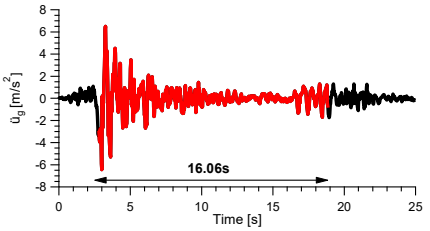

(a) Cape Mendocino

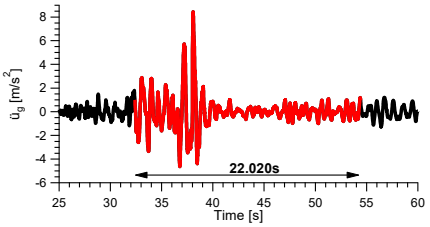

(b) Chi Chi

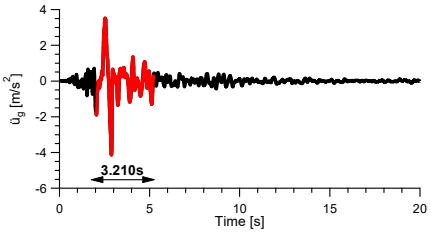

(c) Coyote Lake Comp. 230

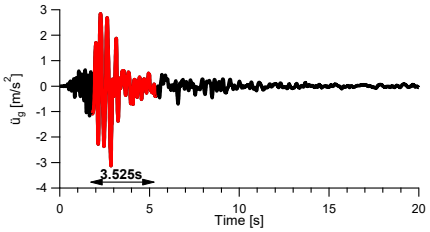

(d) Coyote Lake Comp. 320

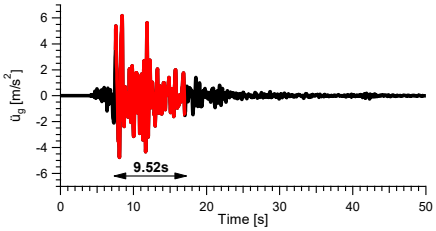

(e) Kobe

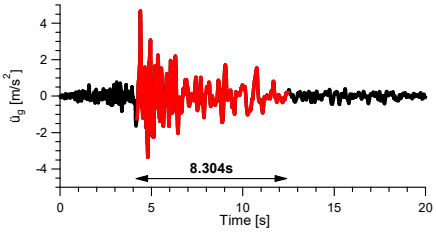

(f) Mendoza

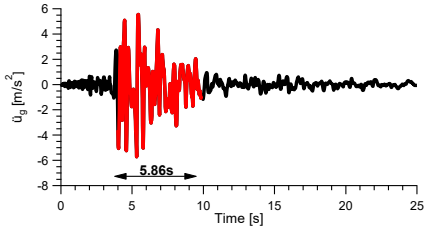

(g) Northridge

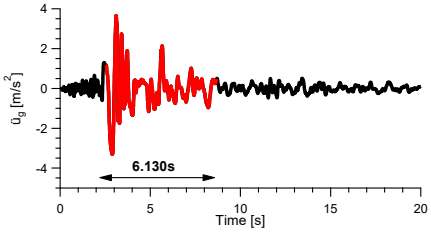

(h) Parkfield

Fig. 17 Earthquake records selected for the analysis

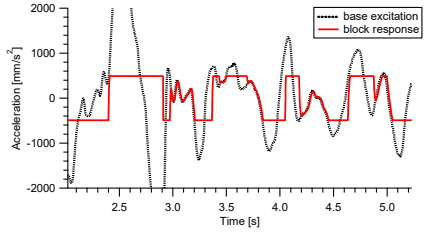

(a) $\Delta t = 0.001\ s$

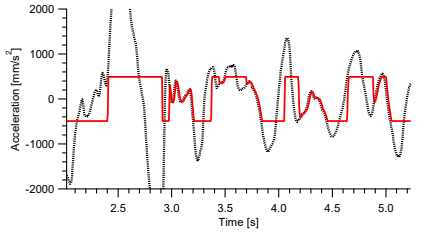

(b) $\Delta t = 0.005\ s$

Fig. 18 Effect of time integration step on acceleration response for Coyote Lake comp. 230, $\mu = 0.050$

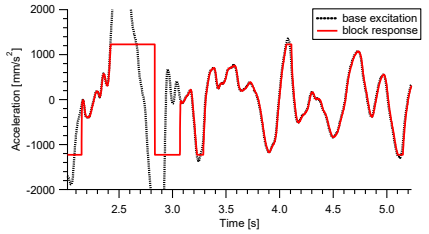

(a) $\Delta t = 0.001\ s$

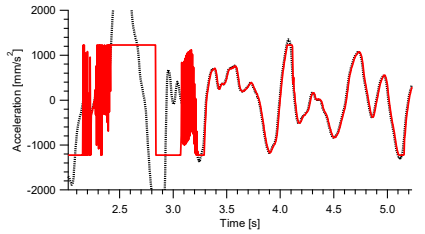

(b) $\Delta t = 0.005\ s$

Fig. 19 Effect of time integration step on acceleration response for Coyote Lake comp. 230, $\mu = 0.125$

(a) $\Delta t = 0.001\ s$ (b) $\Delta t = 0.005\ s$

Fig. 20 Effect of time integration step on acceleration response for Coyote Lake comp. 230, $\mu = 0.20$

Table 6 Result summary for selected records

Event	Comp.	PGA [m/s^2]	$\ddot{u}_{g\,RMS}$ [m/s^2]	$E_{df\,max}$ [J]	μ_{max} [-]
Cape Mendocino	090	6.49	1.923	3.386	0.125
Chi Chi	N	8.44	7.499	9.422	0.175
Coyote Lake	230	4.14	0.295	0.725	0.125
Coyote Lake	320	3.13	0.284	0.455	0.100
Kobe	090	6.18	1.754	5.281	0.150
Mendoza	-	4.68	1.800	0.767	0.075
Northridge	090	5.72	0.078	3.079	0.100
Parkfield	360	3.66	0.408	0.928	0.075

Nonetheless, when evaluating results using the same record with a friction ratio of 0.125 it is possible to note that acceleration time histories for the case with $\Delta t = 0.005\ s$ start exhibiting high frequency stuttering when the block is in stick phase. Fig. 19(b) clearly illustrates this fact. For higher friction ratio values, this effect is further accentuated as can be seen in Fig. 20.

Taking into account this phenomenon, a uniform time integration step of 0.001 s was adopted for all records. Linear interpolation was used for in-between record values.

5.3 Results

Base excitation characterized by the seismic records previously introduced was applied to the computational models with different friction ratios. Special attention was given to energy dissipated by friction, as it is of interest to establish friction coefficients that maximize it.

The different types of energy were computed using the discrete expressions discussed in section in section 2.2.3 of this paper.

Complete results of this study are exhibited in Fig. 21. The main objective was to determine the friction ratios that maximize energy dissipation by friction.

Additionally, the main results are summarized in Table 6. It is important to point out that friction ratios that maximize energy dissipation differ depending on the seismic record. This is reasonable, as each record has different frequency content and, consequently, energy dissipation by friction varies from case to case.

Even though the values specified in Table 6 correspond to the friction ratios for which energy dissipation is absolute maximum, it should be noted that there is a whole range of values for which energy dissipation is almost equal. For example, this friction ratio range comprises values between 0.100 and 0.150 for the Cape Mendocino record. Table 7 presents these ranges for all the selected earthquake records.

At this point, from Table 7, it is important to highlight that a friction coefficient of 0.1 cover most of the seismic records, particularly those with lower significant duration. This recommended value could be very important when selecting contact materials in friction-based seismic isolation systems.

On the other hand, as Calvi and Calvi (2018) point out, higher vertical loads (i.e., higher contact pressures) tend to produce consistently lower friction coefficient values. However, according to Eqs. (18) and (19), the shape and maxima of Fig. 21 do not change with the vertical load, in this case represented by the mass m. For this reason, when vertical loads are high, materials with higher friction coefficients should be selected, to obtain close to 0.1 for these vertical loads.

5.3.1 Relationship between μ_{max} and record's parameters

As a consequence of the variability previously mentioned, it became necessary to relate these friction ratios to base record's intrinsic measures. Two of these record parameters were selected for this analysis: peak ground acceleration (PGA) and root mean square acceleration during motion's significant duration ($\ddot{u}_{g\,RMS}$).

Fig. 22 shows the relationship between peak ground acceleration and the friction ratio that yields maximum energy dissipation. A general tendency can be perceived from this graph: as record's PGA increases, maximum dissipation friction ratio also rises. Note that there are some exceptions to the general tendency just described, though it applies for most cases. The dashed line in Fig. 22 represents a linear approximation of this relationship. This rough calculation can provide a general idea of the friction ratio

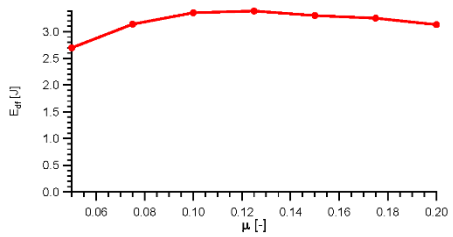

(a) Cape Mendocino

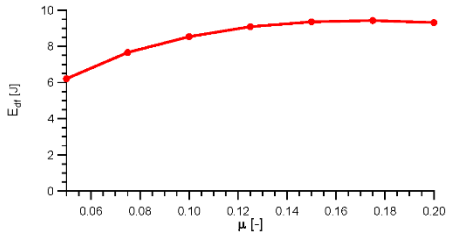

(b) Chi Chi

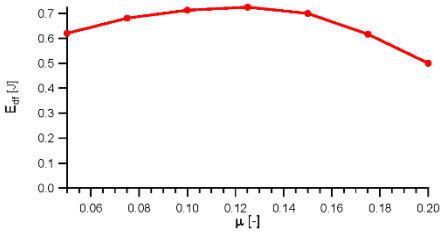

(c) Coyote Lake Comp. 230

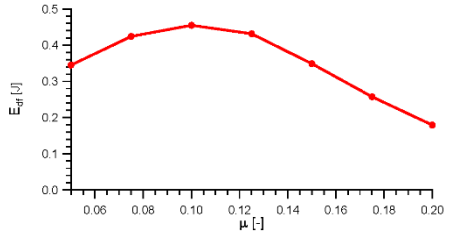

(d) Coyote Lake Comp. 320

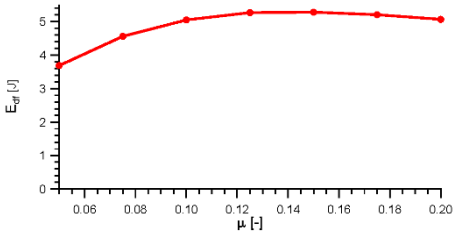

(e) Kobe

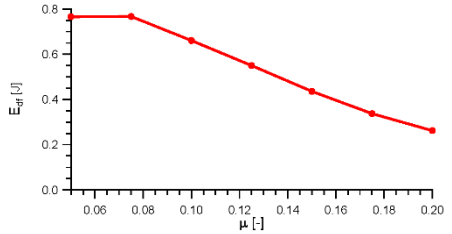

(f) Mendoza

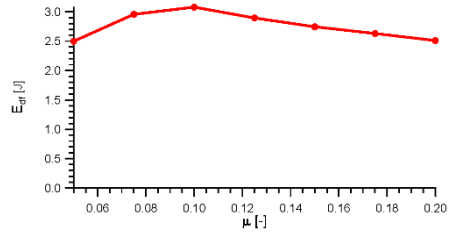

(g) Northridge

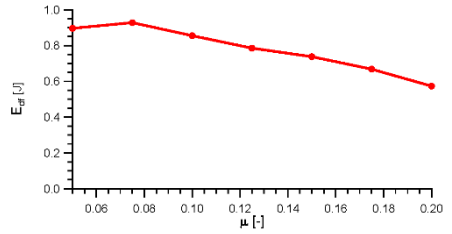

(h) Parkfield

Fig. 21 Friction-dissipated energy v. Friction ratio

Table 7 Suggested range of values for μ_{max}.

Event	Comp.	Range of μ_{max}[-]
Cape Mendocino	090	0.100 - 0.150
Chi Chi	N	0.150 - 0.200
Coyote Lake	230	0.100 - 0.150
Coyote Lake	320	0.075 - 0.125
Kobe	090	0.125 - 0.175
Mendoza	-	0.050 - 0.100
Northridge	090	0.075 - 0.125
Parkfield	360	0.050 - 0.100

that maximizes energy dissipation. However, more earthquake records need to be analyzed in order to verify the proposed expression as the correlation factor r is relatively low.

On the other hand, a clear relationship between record's root mean square acceleration and the friction ratio for which energy dissipation is maximum, could not be

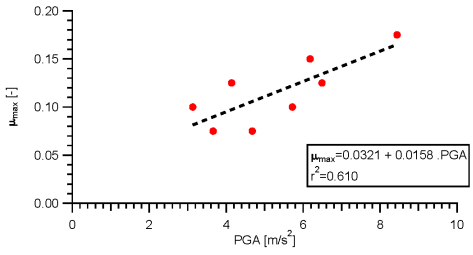

Fig. 22 μ_{max} v. PGA

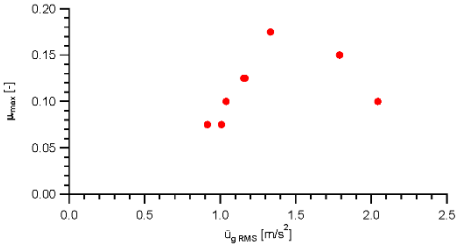

Fig. 23 μ_{max} v. $\ddot{u}_{g\,RMS}$

established. This is illustrated in Fig. 23. From this figure it can be seen that for low values of $\ddot{u}_{g\,RMS}$, friction ratios tended to grow reaching a maximum of 0.175 for a corresponding value of 1.332 m/s^2 (Chi Chi record). Nevertheless, for greater values of acceleration, friction ratios tended to decrease. This was the case for both the Kobe and Northridge records.

5.3.2 Scaling study for a single earthquake record

In order to further elaborate on the findings described in the prior section, the response of the numerical models for a single earthquake record with varying scale factors was analyzed. In this sense, friction ratios that maximize energy dissipation were compared for both the actual record and the upscaled record with peak ground acceleration values of 5.89 m/s^2 ($0.60\,g$), 7.85 m/s^2 ($0.80\,g$) and 9.81 m/s^2 ($1.00\,g$). For this study the Mendoza record was selected. Results are specified in Table 8. From it, it is possible to observe that as the record's scaling factor increases, both dissipated energy and the friction ratio for which it occurs grow.

Fig. 24 shows how friction ratio with maximum dissipated energy vary with peak ground acceleration. It can be seen that for the original record and for the record upscaled to $0.60\,g$, μ_{max} was constant and equal to 0.075. For higher PGA values, friction ratio also increased. This tendency proved true for the record upscaled to both $0.80\,g$ and $1.00\,g$.

In addition, a similar tendency is observed in Fig. 25 for the records' root mean square acceleration.

From the results exhibited in this section, it would appear that friction ratios that maximize energy dissipation tend to increase with both PGA and $\ddot{u}_{g\,RMS}$. Yet this statement should be taken with caution, especially in the case of the record's root mean square acceleration, where there was great variability of μ_{max} depending on the record as showed in Fig. 23.

Regardless, the recommended value of 0.1 seems to cover many different situations.

Table 8 Result summary for the scaling study, Mendoza record

Event	Scale factor	PGA [m/s^2]	$\ddot{u}_{g\,RMS}$ [m/s^2]	$E_{df\,max}$ [J]	μ_{max} [-]
Mendoza	1.00	4.68	0.915	0.767	0.075
	1.26	5.89	1.151	1.217	0.075
	1.68	7.85	1.535	2.108	0.100
	2.10	9.81	1.919	3.237	0.125

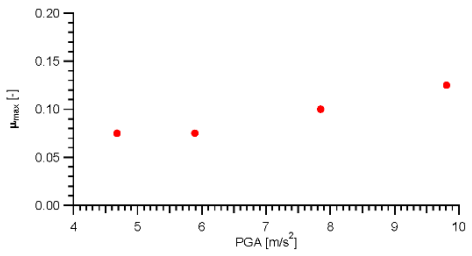

Fig. 24 μ_{max} v. PGA, scaling study for Mendoza record

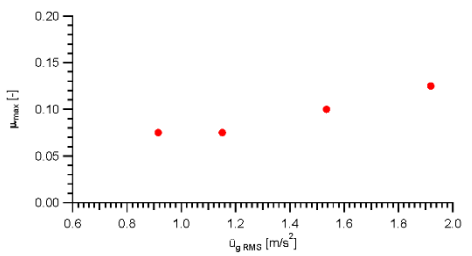

Fig. 25 μ_{max} v. $\ddot{u}_{g\,RMS}$, scaling study for Mendoza record

6. Conclusions

In this paper, friction ratios that maximize energy dissipation for eight different earthquake records were obtained using numerical models of a lead block sliding over a flat surface. These models were experimentally validated with dynamic tests carried out on a shacking table. The conclusions of this study are as follows:

Friction coefficients for which energy dissipation is maximum largely depend on the earthquake record that serves as base excitation. This is demonstrated by the variability that these show with respect to the selected records.

Additionally, it appears that maximum-dissipation friction ratios tend to rise as base excitation's peak ground acceleration also increases. In order to verify this statement, an upscaling study of a single record was carried out. The results of this analysis tend to confirm this tendency. However, it is still not possible to establish a reliable relationship between these two parameters, because as indicated by the linear approximation proposed, correlation factor is low and more cases need to be considered.

It was not possible to establish a clear tendency for the relationship between friction ratios that maximize energy dissipation and the record's root mean square acceleration. According to the cases evaluated on this paper, it would appear that maximum-dissipation friction coefficients increase until they reach a maximum and then, as RMS acceleration increases, they start to decrease.

A friction coefficient of 0.1 can be recommended because cover most of the seismic records, particularly those with lower significant duration. This recommended value could be very important when selecting contact materials in friction-based seismic isolation systems.

Regarding contact interfaces considered for the sliding tests, both interfaces II and IV exhibited friction ratios in the intervals between 0.070 and 0.120. These values seem appropriate and close to the ones that maximize energy dissipation determined with the computational models. Consequently, one of these two interfaces should be adopted in order to maximize energy dissipation by friction of a block sliding on a flat surface subjected to earthquake excitation.

The results obtained are valid for friction-based seismic isolation systems with flat sliding bearings.

Acknowledgments

The authors would like to thank Dr. Martín Domizio and Mr. Gabriel Houri for their help in setting up and carrying out the dynamic tests. Financial support from CONICET, Universidad Nacional de Cuyo and Universidad Nacional de Tucumán is greatly appreciated.

References

ANSYS, I. (2010), Theory reference, Canonsburg: ANSYS, Inc.

Arias, A. (1970), "A measure of earthquake intensity", In: *Seismic Design for Nuclear Power Plants* (Ed.: Hansen, R.J.), Massachusetts Institute of Technology Press, Cambridge, MA, USA.

Calvi, P.M. and Calvi, G.M. (2018), "Historical development of friction-based seismic isolation systems", *Soil Dyn. Earthq. Eng.*, **106**, 14-30. https://doi.org/10.1016/j.soildyn.2017.12.003

Den Hartog, J.P. (1931), "Forced vibrations with combined Coulomb and viscous friction", *Transact. Am. Soc. Mech. Engr.*, **53**(1931), 107-115.

Etedali, S., Akbari, M. and Seifi, M. (2019), "MOCS-based optimum design of TMD and FTMD for tall buildings under near-field earthquake including SSI effects", *Soil Dyn. Earthq. Eng.*, **119**(2019), 36-50. https://doi.org/10.1016/j.soildyn.2018.12.027

Hundal, M.S. (1979), "Response of a base excited system with Coulomb and viscous friction", *J. Sound Vib.*, **64**(1979), 371-378. https://doi.org/10.1016/0022-460X(79)90583-2

Inaudi, J.A. and Kelly, J.M. (1995), "Mass damper using friction-dissipating devices", *J. Eng. Mech.*, **121**(1), 142-149. https://doi.org/10.1061/(ASCE)0733-9399(1995)121:1(142)

Jiang, J., Ho, S.C.M, Markle, N.J., Wang, N. and Song, G. (2019), "Design and control performance of a frictional tuned mass damper with bearing-shaft assemblies", *J. Vib. Control*, **25**(12), 1812-1822. https://doi.org/10.1177/1077546319832429

Kim, S.Y. and Lee, C.H. (2019), "Peak response of frictional tuned mass damper optimally designed to white noise base acceleration", *Mech. Syst. Signal Process.*, **117**(2019), 319-332. https://doi.org/10.1016/j.ymssp.2018.08.003

Lee, S.K., Park, J.H., Moon, B.W., Min, K.W., Lee, S.H. and Kim, J. (2008), "Design of a bracing-friction damper system for seismic retrofitting", *Smart Struct. Syst., Int. J.*, **4**(5), 685-696. https://doi.org/10.12989/sss.2008.4.5.685

López, I., Busturia, J. and Nijmeijer, H. (2004), "Energy dissipation of a friction damper", *J. Sound Vib.*, **278**(2004), 539-561. https://doi.org/10.1016/j.jsv.2003.10.051

Nims, D.K., Richter, P.J. and Bachman, R.E. (1993), "The use of the energy dissipating restraint for seismic hazard mitigation", *Earthq. Spectra*, **9**(3), 467-489. https://doi.org/10.1193/1.1585725

Ontiveros-Pérez, S.P., Miguel, L.F.F. and Riera, J.D. (2019), "Reliability-based optimum design of passive friction dampers in buildings in seismic regions", *Eng. Struct.*, **190**, 276-284. https://doi.org/10.1016/j.engstruct.2019.04.021

Ozbulut, O. and Silwal, B. (2016), "Performance assessment of buildings isolated with S-FBI system under near-fault earthquakes", *Smart Struct. Syst., Int. J.*, **17**(5), 709-724. https://doi.org/10.12989/sss.2016.17.5.709

Pall, A.S., Marsh, C. and Fazio, P. (1980), "Friction joints for seismic control of large panel structures", *J. Prestress. Concrete Inst.*, **25**(6), 38-61. https://doi.org/10.15554/pcij.11011980.38.61

Ricciardelli, F. and Vickery, B.J. (1999), "Tuned vibration absorbers with dry friction damping", *Earthq. Eng. Struct. Dyn.*, **28**(7), 707-723. https://doi.org/10.1002/(SICI)1096-9845(199907)28:7<707::AID-EQE836>3.0.CO;2-C

Shahbazi, P. and Taghikhany, T. (2017), "Sensitivity analysis of variable curvature friction pendulum isolator under near-fault ground motions", *Smart Struct. Syst., Int. J.*, **20**(1), 23-33. https://doi.org/10.12989/sss.2017.20.1.023

Shen, S., Pan, P., Sun, J., Gong, R., Wang, H. and Li, W. (2017), "Development of a double-sliding friction damper (DSFD)", *Smart Struct. Syst., Int. J.*, **20**(2), 151-162. https://doi.org/10.12989/sss.2017.20.2.151

Trifunac, M. and Brady, A. (1975), "A study on the duration of strong earthquake ground motion", *Bull. Seismol. Soc. Am.*, **65**(3), 581-626.

Uang, C.M. and Bertero, V. (1990), "Evaluation of seismic energy in structures", *Earthq. Eng. Struct. Dyn.*, **19**(1990), 77-90. https://doi.org/10.1002/eqe.4290190108

Yang, J., Li, J.B. and Lin, G. (2006), "A simple approach to integration of acceleration data for dynamic soil-structure interaction analysis", *Soil Dyn. Earthq. Eng.*, **26**(2006), 725-734. https://doi.org/10.1016/j.soildyn.2005.12.011

Zahraei, S.M., Moradi, A. and Moradi, M. (2013), "Using Pall friction dampers for seismic retrofit of a 4-story steel building in Iran", In: *Topics in Dynamics of Civil Structures*, Volume 4, Springer, New York, NY, USA.

FC